

# Lithium, rotation and metallicity in the open cluster M35

D. Cuenda-Muñoz<sup>1,\*</sup>, D. Barrado<sup>1</sup>, M. A. Agüeros<sup>2,3</sup>, J. L. Curtis<sup>2</sup>, and H. Bouy<sup>3,4</sup>

<sup>1</sup> Centro de Astrobiología (CAB), CSIC-INTA, ESAC Campus, Camino Bajo del Castillo s/n, 28692, Villanueva de la Cañada, Madrid, Spain

<sup>2</sup> Department of Astronomy, Columbia University, 550 West 120th Street, New York, NY 10027, USA

<sup>3</sup> Laboratoire d'astrophysique de Bordeaux, Univ. Bordeaux, CNRS, B18N, Allée Geoffroy Saint-Hilaire, 33615 Pessac, France

<sup>4</sup> Institut Universitaire de France (IUF), Paris, France

Received April 03, 2024; accepted May 04, 2024

## ABSTRACT

**Context.** Lithium (Li) abundance is an age indicator for G, K, and M stellar types, as its abundance decreases over time for these spectral types. However, despite all of the observational efforts made over the past few decades, the role of rotation, stellar activity, and metallicity in the depletion of Li is still unclear.

**Aims.** Our purpose is to investigate how Li depletion is affected by rotation and metallicity in G and K members of the roughly Pleiades-aged open cluster M35.

**Methods.** We have collected an initial sample of 165 candidate members observed with the WIYN/Hydra spectrograph. In addition, we have taken advantage of three previous spectroscopic studies of Li in M35. As a result, we have collected a final sample of 396 stars observed with the same instrument, which we have classified as non-members, possible non-members, possible members, and probable members of the cluster. We have measured iron abundances, Li equivalent widths, and Li abundances for the 110 M35 members added to the existing sample by this study. Finally, rotation periods for cluster members have been obtained from the literature or derived from Zwicky Transient Facility light curves.

**Results.** We have confirmed that fast G and K rotators are Li-rich in comparison with slow rotators of similar effective temperature. This trend, which is also seen in previous studies, is more evident when binaries are not taken into account. Furthermore, while we derived an average metallicity of  $[Fe/H] = -0.26 \pm 0.09$  from our spectra, the distribution of Li in M35 is similar to those observed for the Pleiades and M34 open clusters, which have solar metallicity and slightly different ages. In addition, we have shown that an empirical relationship proposed to remove the contribution of the Fe I line at 670.75 nm to the blended feature at 670.78 nm overestimates by 5–15 mÅ the contribution of this iron line for M35 members.

**Conclusions.** M35 fast G and K rotators have depleted less Li than their slower counterparts. Furthermore, a 0.2–0.3 dex difference in metallicity appears to make little difference in the Li distributions of open clusters with ages between 100 and 250 Myr.

**Key words.** stars: late-type – open clusters and associations : individual (M35, NGC 2168) – stars: rotation – stars: abundances

## 1. Introduction

As lithium (Li) is gradually destroyed in the interiors of solar-like F, G, and K main-sequence (MS) stars, the abundance of this element can be used as an age indicator for these stars. In addition, as the internal structure of the star has a strong influence on the depletion of Li, the study of the dependence of Li abundance on spectral type and age provides a useful tool for improving stellar evolutionary models.

Li depletion is driven by convection, but additional factors play an important role in this process. For example, evidence of the connection between stellar rotation and Li depletion was found in the 1990s, when Soderblom et al. (1993) revealed that the slow rotators in the Pleiades (125 Myr old) were Li-poor compared to the fast ones. As this discovery contradicted predictions, many stellar associations have been observed in the decades since, and several different explanations have been proposed to account for this unexpected result.

Siess & Livio (1997) linked rotation and Li depletion through the mixing length parameter  $\alpha$ . A smaller  $\alpha$  would imply a thinner convective envelope and, consequently, a reduction in the amount of Li that is destroyed. If  $\alpha$  scales with the inverse of the angular velocity, rapid rotators would be richer in Li than slow rotators. On the other hand, Bouvier (2008) proposed that the star-disk interaction, known as disk locking, that takes place during the early pre-main sequence (PMS) enhances differential rotation, preventing the star from spinning up. Consequently, a longer disk lifetime should result in a slower rotator that will reach the zero-age-main-sequence (ZAMS) with less Li due to this externally enforced rotational mixing.

Multiple authors have studied the observed evolution of the Li–rotation connection from the PMS to the ZAMS. Bouvier et al. (2016) investigated this relationship in the 5-Myr-old, star-forming region NGC 2264, and demonstrated that the Li overabundance is detected in fast rotators even at this early stage of stellar evolution. Barrado et al. (2016) and Bouvier et al. (2018) confirmed the tight Li–rotation connection in the Pleiades, and Arancibia-Silva et al. (2020) also demonstrated its existence in the 125-Myr-old Psc-Eri stellar stream. These studies indicate

\* dcuenda@cab.inta-csic.es

that the Li overabundance increases during the PMS: Li abundance in fast rotators is 120% the Li abundance in slow rotators at 5 Myr, and it reaches 600% on the ZAMS, which is the evolutionary status of K dwarfs at the age of the Pleiades.

An additional consideration is the magnetic activity in these stars. Somers & Pinsonneault (2014, 2015) suggested that strong magnetic activity inflates the radius of young stars, reducing the temperature at the base of the convective envelope and, consequently, limiting PMS Li depletion. If fast rotators have stronger magnetic fields than slow ones, their Li abundance will consequently be higher. In this context, it is worth noting that while it is generally accepted that the observed Li spread for a given mass corresponds to real abundance differences, Barrado et al. (2016, and references therein) proposed that the Li overabundance in fast rotators is partially an observational effect from increased activity in these stars.

Finally, metallicity also influences Li depletion: stars with lower metallicity have thinner convective envelopes and, consequently, their Li depletion is less efficient. This anti-correlation between metallicity and Li depletion has recently been confirmed for solar analogs by Martos et al. (2023), strengthening the models proposed by Castro et al. (2009) and Dumont et al. (2021).

To completely understand the role that age, activity, rotation, and metallicity play in Li depletion, it is crucial to have a reliable and extensive set of observations of MS FGK stars. As the members of open clusters share the same age and metallicity, they constitute the perfect targets for these observations. Our focus is on the open cluster M35 (NGC 2168), a rich (Barrado y Navascués et al. 2001b; Bouy et al. 2015), relatively distant (885 pc; Jeffries et al. 2021) cluster that is often thought of as a much richer analog of the Pleiades.

Jeffries et al. (2021) have investigated the Li–rotation connection for G and K members of M35, finding a strong correlation between the equivalent width of the Li line, EW(Li), rotation, and radius inflation. However, the position of the cluster in the age–metallicity plane is still ambiguous: while Jeffries et al. (2021) quote an age of  $140 \pm 15$  Myr, Abdelaziz et al. (2022) derived an age of 126 Myr for M35, closer to that of the Pleiades. More significantly, only a few authors have provided values for M35’s metallicity: Barrado y Navascués et al. (2001a) and Steinhauer & Deliyannis (2004) found sub-solar values ( $[Fe/H] = -0.21 \pm 0.10$  and  $-0.143 \pm 0.014$ , respectively), while, based on their measurements of the EW of the Ca I line for stars in their sample, Anthony-Twarog et al. (2018) assumed a solar metallicity for the cluster.

In this paper, we present our analysis of unpublished spectra and new light curves, with which we have expanded the sample of M35 members with EW(Li) and rotation period measurements presented in Jeffries et al. (2021). In addition, we derive the metallicity of M35 by analyzing the spectra collected for a sample of single GK dwarfs with very high probability of being cluster members. Finally, we have compared our results for M35 to those for the Pleiades and for M34, another open cluster with an age quite similar to that of M35.

In Section 2, we present our spectroscopic sample, obtained with multiple nights of observations using the Hydra spectrograph on the 3.5-m telescope, WIYN Observatory, Kitt Peak, USA.<sup>1</sup> We also describe other WIYN/Hydra M35 campaigns

whose results were incorporated into this study. In Section 3, we describe our efforts to finalize a membership catalog for M35, and to distinguish between candidate single and candidate binary members of the cluster. In Section 4, we discuss our sample of rotational period measurements for the members of M35. This includes new rotation periods obtained from our analysis of Zwicky Transient Facility (ZTF; Masci et al. 2019) light curves, as well as periods from the literature. Section 5 explains the method employed to obtain effective temperatures and luminosities for the members of M35, and describes the analysis carried out to derive the metallicity of this cluster and provide new Li measurements. Finally, the results obtained are presented and discussed in Section 6, and we provide our conclusions in Section 7.

## 2. Assembling our spectroscopic sample

Our sample is made up of M35 candidate members observed with the Hydra multifiber spectrograph. Hydra has more than 80 fibers with which one can cover a field 60 arcminutes in diameter. Since half of M35’s members are contained within a diameter of less than 40 arcminutes (Cantat-Gaudin & Anders 2020), Hydra is able to observe most of the cluster within a single observation. The light collected by each fiber is transmitted to the bench spectrograph and scattered by the selected grating. Two different science cables are available for each configuration of fibers, the red one covering 400–1100 nm and the blue covering 300–800 nm.

### 2.1. Previously unpublished Hydra spectra

Over the course of four observational campaigns between 1998 January and 2001 March, more than 300 M35 candidate members were observed with Hydra. Here we focus on the two campaigns with unpublished data. From 1999 December 12–15, eight science images were taken using the blue Hydra fiber cable, each with the same configuration of 17 sky fibers and 76 science fibers. From 2001 February 22–23, five science images were taken using the same fiber cable, but the configuration was slightly different: there were five sky fibers and 89 science fibers. None of the sources observed in 1999 was observed again in 2001 February. Table 1 lists the dates of the observations, the central coordinates, and the exposure times for each image.

We reduced the 165 stellar spectra obtained as follows. For homogeneity with previous studies with Hydra (section 2.2), we used standard IRAF<sup>2</sup> tools to obtain the smoothed and continuum-normalized spectrum corresponding to each source in each of the images. First, we smoothed the spectra taken during each exposure using the boxcar task included in the images.imfilter package. Second, we removed the continuum by fitting a cubic spline function to each spectrum taking advantage of the continuum task included in noao.onedspec. Finally, we employed the scopy task in imred.hydra to extract the individual (smoothed and continuum normalized) spectrum for each observed source. Each of the resulting  $R \approx 20,000$  spectra covers

due University. The astronomical community is honored to have the opportunity to conduct astronomical research on Iolkam Du’ag (Kitt Peak) in Arizona. We recognize and acknowledge the very significant cultural role and reverence that this site has to the Tohono O’odham Nation.

<sup>2</sup> IRAF is distributed by the National Optical Astronomy Observatories, which are operated by the Association of Universities for Research in Astronomy, Inc., under cooperative agreement with the National Science Foundation.

<sup>1</sup> The WIYN Observatory is a joint facility of the NSF’s National Optical-Infrared Astronomy Research Laboratory, Indiana University, the University of Wisconsin-Madison, Pennsylvania State University, the University of Missouri, the University of California-Irvine, and Pur-

**Table 1.** Science exposures taken during the December 1999 and February 2001 WIYN/Hydra campaigns. Date, central coordinates, and exposure time are shown for each exposure.

Image	$\alpha(2000)$ hh:mm:ss	$\delta(2000)$ dd:mm:ss	Date	Exposure Time (s)
N2017	06:09:06.0	24:20:42	1999 Dec 12	4355
N2018	06:09:06.1	24:20:42	1999 Dec 12	7200
N2019	06:09:06.1	24:20:42	1999 Dec 12	7200
N2020	06:09:06.1	24:20:42	1999 Dec 12	4920
N3033	06:09:06.0	24:20:42	1999 Dec 13	7200
N3034	06:09:06.0	24:20:42	1999 Dec 13	4500
N4049*	06:09:06.0	24:20:42	1999 Dec 14	2725
N5036	06:09:06.0	24:20:42	1999 Dec 15	6300
N1033	06:09:04.4	24:18:48	2001 Feb 22	7200
N1034	06:09:04.4	24:18:48	2001 Feb 22	7200
N1036	06:09:04.4	24:18:48	2001 Feb 22	7800
N2099	06:09:04.4	24:18:48	2001 Feb 23	7200
N2100	06:09:04.4	24:18:48	2001 Feb 23	9000

\*We used N4049 to derive RVs, but not to measure Li EWs.

the wavelength interval between 640 and 690 nm. The Li doublet at 670.78 nm is included in this range as well as a number of iron lines.

## 2.2. Previously published spectra from these campaigns

We also included in our sample the G and K dwarfs observed in the two other observing campaigns from that same time period and analysed in previous publications (Barrado y Navascués et al. 2001a; Anthony-Twarog et al. 2018). Although these authors address the Li–rotation connection, they rely on rotation velocities, which are affected by the uncertainty in the rotation inclination angle, in contrast to the analysis provided in this work, which relies on measurements of rotation periods.

Barrado y Navascués et al. (2001a) observed 76 candidate members of M35 selected from the photometric survey of the cluster of Barrado y Navascués et al. (2001b). Anthony-Twarog et al. (2018) acquired spectra of 85 stars, 77 of which had preliminary radial velocities (RVs) consistent with membership; the other eight were selected based on their positions in a color-magnitude diagram (CMD). There is no overlap between the objects analysed in the aforementioned studies, but a few of them were also observed in 1999 December and 2001 February. Fifteen of the spectra presented in this work are for stars also observed by Barrado y Navascués et al. (2001a), and five are also included in Anthony-Twarog et al. (2018).

## 2.3. Other Hydra surveys of M35

Jeffries et al. (2021) employed Hydra to observe 342 candidate members of M35 selected from the catalogs of Bouy et al. (2015), Meibom et al. (2009), and Libralato et al. (2016). Jeffries et al. (2021) rejected 100 of these stars because they considered them non-members of the cluster, found no rotation periods for them, or these objects exhibited a poor fit when analysed with the Virtual Observatory Spectral Energy Distribution (SED) Analyser (VOSA; Bayo et al. 2008). Because we developed our own set of membership criteria, and have a different set of rotation period measurements for our analysis, we have incorporated these 100 discarded stars into our sample (ten were observed as part of our program).

**Table 2.** Summary of our complete sample in terms of the origin of the data.

Campaign	Number of Sources	Authors
1998 January	76	Barrado y Navascués et al. (2001a)
1999 December	76	This Work
2001 February	89	This Work
2001 March	85	Anthony-Twarog et al. (2018)
2017 November	100	Jeffries et al. (2021)

On the other hand, the 242 stars that were analyzed by Jeffries et al. (2021) have not been included in our sample for re-analysis. Instead, we incorporated the Jeffries et al. (2021) results for these stars into our analysis in section 6. It is worth mentioning that 115 of these stars are included in Barrado y Navascués et al. (2001a), Anthony-Twarog et al. (2018), or the Hydra campaigns presented in this work.

## 2.4. The complete sample

As shown in Table 2, our sample includes 76 stars taken from Barrado y Navascués et al. (2001a), 85 taken from Anthony-Twarog et al. (2018), 100 taken from Jeffries et al. (2021), and 165 stars added by this study. As a result, we obtained a final sample of 396 unique G and K candidate members of M35 for which we could obtain or have Li measurements. The complete sample is presented in Table 3.

## 3. Revisiting the membership and multiplicity of stars in our sample

### 3.1. An initial membership selection based on Bouy et al. (2015) and our own proper-motion analysis

Using TOPCAT (Taylor 2005), we cross-matched our 396 stars with the *Gaia* Data Release 3 (DR3; Gaia Collaboration et al. 2023), obtaining astrometry and photometry for 395 candidate members (see the CMD in the left panel, Figure 1). We also cross-matched our catalog with that of Bouy et al. (2015), as these authors provided an extensive membership analysis for M35. We found counterpart for 373 stars in that work.

We then used Clusterix 2.0, a Spanish Virtual Observatory tool (Balaguer-Núñez et al. 2020), to assign membership probabilities to our candidates based on their *Gaia* Early Data Release 3 (EDR3; Gaia Collaboration et al. 2021) proper motions.<sup>3</sup> After selecting a region of the sky including M35 and a region free of cluster members, Clusterix 2.0 uses a non-parametric method to distinguish the proper-motion distribution of the cluster members and that of the field stars. In this process, the number of cluster members,  $N_c$ , is estimated, and the membership probability of each star in the selected regions is computed.

Clusterix 2.0 returns a file that includes, for each star considered, the *Gaia* EDR3 photometry and astrometry and a membership probability. In addition, the  $N_c$  stars with the highest membership probabilities are flagged as members of the cluster. We removed from this preliminary list of candidate members around half of them due to the large uncertainties in the photometry and/or astrometry measured for those stars, or because their parallaxes and/or proper motions were very different from those of M35 (Gaia Collaboration et al. 2018).

<sup>3</sup> Clusterix 2.0 does not yet include DR3 proper motions.

**Table 3.** Cross-identification numbers, coordinates, and observation campaigns for the complete sample presented in this work. Our sample is composed of 396 stars. Columns  $\alpha$  and  $\delta$  indicate the coordinates employed for the pointing. For the stars that have a counterpart in [Anthony-Twarog et al. \(2018\)](#) and/or [Jeffries et al. \(2021\)](#), we have also included the corresponding IDs in these papers. This table is only partially presented. Its complete version is available electronically.

ID <sup>a</sup>	$\alpha$ (2000) hh:mm:ss	$\delta$ (2000) dd:mm:ss	$\alpha$ (2000) deg	$\delta$ (2000) deg	Campaign	AT18 <sup>b</sup> ID	Je21 <sup>c</sup> ID
5076	06:08:52.9	+24:17:20	92.22042	24.28889	2001 Mar	16010	–
5081	06:09:26.200	+24:29:03.0	92.35917	24.48417	1998 Jan	–	–
7117	–	–	92.22672	24.05225	2017 Nov	–	J06085441+2403081
7036	06:09:00.7	+24:35:53	92.25292	24.59806	2001 Feb	–	–
5373	06:08:49.270	+24:15:33.30	92.20529	24.25925	1999 Dec	–	–
...	...	...	...	...	...	...	...

**Notes.** As the 20 objects in common between the campaigns analysed in this work and the ones presented in [Barrado y Navascués et al. \(2001a\)](#) and [Anthony-Twarog et al. \(2018\)](#) are shown as different rows with the same identification number, the table includes 416 rows. <sup>(a)</sup> Object IDs between 5000 and 7000 are taken from [Barrado y Navascués et al. \(2001b\)](#). The stars not found in that catalog have been labelled with numbers between 7000 and 8000. <sup>(b)</sup> AT18 is [Anthony-Twarog et al. \(2018\)](#). <sup>(c)</sup> Je21 is [Jeffries et al. \(2021\)](#).

We then combined the membership probabilities of [Bouy et al. \(2015\)](#) with those derived by Clusterix 2.0 to classify each star as a non-member, a possible non-member, a possible member, or a probable member.

We flagged as non-members stars whose membership probabilities were below 50% in [Bouy et al. \(2015\)](#) and that were also rejected as members after running Clusterix 2.0. In addition, visual inspection of the cluster CMDs allowed us to identify 16 stars as photometric non-members. The stars that had a counterpart in either [Bouy et al. \(2015\)](#) or Clusterix 2.0, but not in both, and whose membership probabilities did not meet our requirements, were classified as possible non-members, as were stars that did not have a counterpart in either of them.

We classified as possible members the stars that were considered members by [Bouy et al. \(2015\)](#), that is, their membership probabilities were  $\geq 50\%$ , or after running Clusterix 2.0, but not by both. Finally, we classified as probable members the stars that met both requirements.

In this manner, we identified 101 stars in our original sample of 396 as non-members (26%), 44 stars as possible non-members (11%), 129 stars as possible members (32%), and 122 as probable members (31%) of M35. In our catalog, presented in Table 4, we use the labels *NM*, *CMD NM*, *NM?*, *Poss*, and *Prob* to indicate these membership categories.

### 3.2. Measuring radial velocities and distinguishing between single and binary stars in our sample

#### 3.2.1. Measuring radial velocities from our Hydra data

We employed iSpec, described in [Blanco-Cuaresma et al. \(2014\)](#), to measure radial velocities (RVs) for the M35 candidate members observed during the 1999 December and 2001 February campaigns. First, each spectrum was transformed to the solar barycentric reference frame. We then derived the RV by cross-correlating the spectrum with a solar mask covering the wavelength range 372–926 nm. We obtained eight measurements of the RV for the M35 candidates observed in 1999 and five measurements for those observed in 2001.

We used these RVs to distinguish between spectroscopic binaries and single stars by employing an approach similar to that of [Leiner et al. \(2015\)](#). The standard deviation in RV ( $e$ ) for each star was compared with the maximum and the minimum single-measurement precision in RV calculated by iSpec for that star ( $max(i)$  and  $min(i)$ , respectively).

The stars whose ratios  $e/max(i)$  and  $e/min(i)$  were both  $< 4$  were considered single, while those whose standard deviation in RV was clearly above the single-measurement precision derived for any of their spectra were classified as SBs. The M35 candidates with  $e/max(i) < 4$  but  $e/min(i) \geq 4$  were classified as having an unknown multiplicity.

In addition, the average RV of each single star was calculated to distinguish between single members and single non-members of the cluster. We considered single members those stars whose average RVs fall within the interval  $[V_{rad} - 3\sigma, V_{rad} + 3\sigma]$ , where  $V_{rad}$  and  $\sigma$  were taken from [Gaia Collaboration et al. \(2018\)](#):  $V_{rad} = -7.70 \text{ km s}^{-1}$ ;  $\sigma = 0.27 \text{ km s}^{-1}$ .

We added a “–” symbol to the membership labels employed for the non-members and possible non-members in our sample that were also considered single non-members based on their RVs. Conversely, we added a “+” to the membership labels for the possible and probable members whose RVs indicate that they are single members of M35.

#### 3.2.2. Using Gaia data and the literature to distinguish between single and binary stars

*Gaia* DR3 and previous studies of M35 provided other avenues for identifying single and binary members of the cluster, particularly for those stars for which we did not obtain our own Hydra spectra. The *Gaia* Renormalised Unit Weight Error (RUWE) is expected to be  $\leq 1.0$  for sources when the single-star model gives a good fit to the astrometric observations, and previous studies have found that larger RUWE values imply that the objects are unresolved binaries in wide orbits (e.g., [Deacon & Kraus 2020](#); [Ziegler et al. 2020](#); [Kervella et al. 2022](#)). Accordingly, we flagged as wide binaries the 41 stars in our sample whose  $RUWE > 1.2$ .

We also took advantage of the membership classification published in [Barrado y Navascués et al. \(2001a\)](#) for the 76 M35 candidate members observed by these authors. After analyzing the RVs they measured, these authors split their sample into single members (39 stars), spectroscopic binary members (13), and non-members (24). We employed these labels for the part of the sample taken from that work but we kept the classification described in the previous section for the 15 stars observed in 1999 December and 2001 February that are included in [Barrado y Navascués et al. \(2001a\)](#). Six of these 15 dwarfs are members of M35.

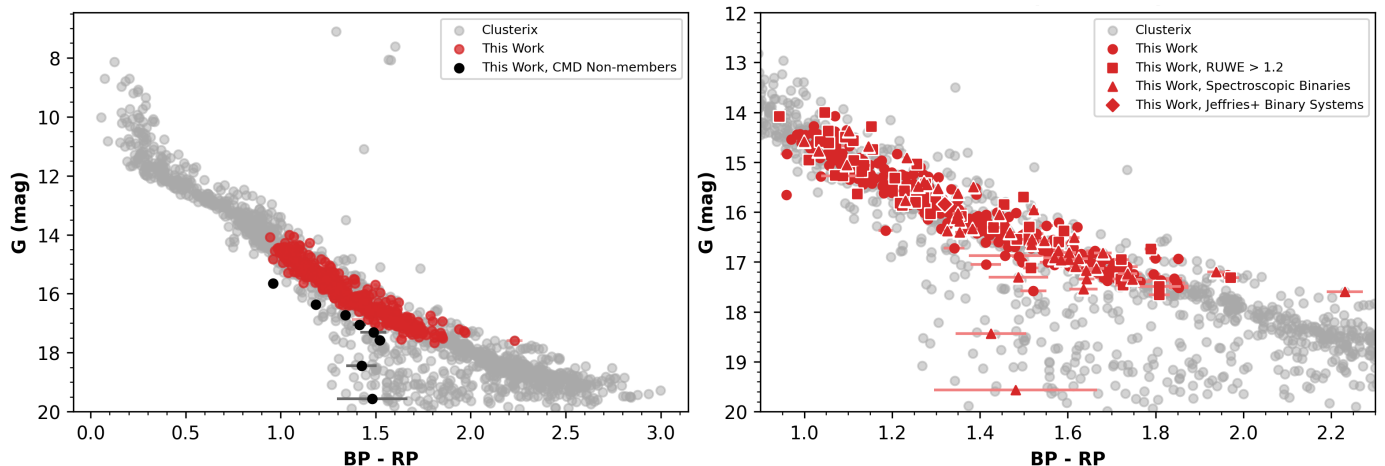


**Fig. 1.** *Gaia* DR3 CMD for M35. *Left*—The grey points represent stars in the vicinity of M35 that Clusterix 2.0 classified as cluster members. We have carried out a subsequent analysis removing some stars whose parallaxes and/or proper motions were very different from those of M35 (Gaia Collaboration et al. 2018). Candidate members of the cluster in our sample are shown in red, while the black circles are stars whose photometry suggests they are not members of M35. We used optical and infrared photometry published in Bouy et al. (2015) to classify eight other photometric outliers as non-members. *Right*—A zoomed-in version of the CMD highlighting the multiple systems in our sample. The squares are potential wide binaries identified by *Gaia*, triangles are spectroscopic binaries, and diamonds are binary systems found by Jeffries et al. (2021). Note that neither CMD has been corrected for reddening.

As a further verification of our membership scheme, we cross-matched our complete sample with the catalog of Leiner et al. (2015), finding counterparts for 174 of the 396 stars. Reassuringly, the 28 stars that we classify as single members that have counterparts in Leiner et al. (2015) are also M35 members in that work. We turned to the binary / single star classification provided by Leiner et al. (2015) only for the part of the sample taken from Anthony-Twarog et al. (2018) and the part recovered from Jeffries et al. (2021).

At the end of this process, we had the sample of 41 wide binaries determined from their RUWE values, and another 46 stars identified as spectroscopic binaries thanks to the RV analysis discussed. One more binary system in our sample was identified from checking the list of probable binary systems defined by Jeffries et al. (2021). In total, we therefore found that 88 of the 396 candidates members that composed our sample could be considered binaries. These 88 binaries are represented by squares, triangles, and diamonds in the CMD shown in the right panel of Figure 1, and are indicated with binary flag = 1 in Table 4.

### 3.3. Summary

As mentioned above, we removed 16 candidates from our sample after visual inspection of their position in several CMDs. Eighty-five other stars were discarded because the membership probabilities derived by Bouy et al. (2015) and the analysis carried out with Clusterix 2.0 both labeled them as non-members. Reassuringly, 28 of these 85 candidates (labeled with *NM*- in Table 4) have RVs incompatible with M35 membership. Similarly, 17 of the 44 stars classified as possible non-members have RVs incompatible with cluster membership. These 17 dwarfs are labeled with *NM*?- in Table 4.

On the other hand, we identified 129 dwarfs as possible members. The RVs confirmed 61 of these candidates as cluster members (labeled with *Poss+* in Table 4). In addition, our sample includes 122 M35 probable members, of which 68 (labeled with *Prob+* in Table 4) are single stars with RVs consistent with that of the cluster. Hereafter, we refer to the combined list of

**Table 4.** Membership class and binary status for the complete sample presented in this work. Our sample is composed of 396 stars. This table is only partially presented. Its complete version is available electronically.

ID	RV Class <sup>a</sup>	RV Source <sup>b</sup>	Final Memb. Class	Binary Flag <sup>c</sup>
5076	SM	L15	Poss+	0
5081	SB1	B01	NM	1
7117	BM	L15	Prob	1
7036	SM	This Work	Prob+	0
5373	U	This Work	CMD NM	0
...	...	...	...	...

**Notes.** <sup>(a)</sup> *MEM* and *SM* account for single members; *NM* and *SN* account for single non-members; *SB*, *BLM*, *BLN*, *BM*, *BN*, *BU*, *SB1*, and *SB2* account for spectroscopic binaries; and *U* accounts for unknown multiplicity. <sup>(b)</sup> B01 is Barrado y Navascués et al. (2001a) and L15 is Leiner et al. (2015). <sup>(c)</sup> 1 = likely binary, 0 = single star.

251 possible and probable members we obtained as members of M35.

## 4. Assembling our sample of rotation periods

We cross-matched our sample of 251 cluster members with the photometric surveys of Meibom et al. (2009), Nardiello et al. (2015), Libralato et al. (2016), and Soares-Furtado et al. (2020). In addition, new rotation periods were derived by analyzing the light curves obtained from Zwicky Transient Facility (ZTF; Masci et al. 2019) data. The main properties of these photometric surveys are shown in Table 5.

### 4.1. Rotation periods from the literature

Our primary source of literature periods is the survey of Meibom et al. (2009), who mixed high-frequency observations over the course of about two weeks with low-frequency observations over nearly five months to measure periods for both fast and slow

**Table 5.** Field of view, instrument characteristics, timespan, and cadence for the photometric surveys from which we obtained rotation periods for our sample.

Authors	Telescope	Field of View	Plate scale (arcsec/pixel)	Timespan	Cadence
Meibom et al. (2009)	WIYN 0.9 m (Kitt Peak Observatory)	$\approx 20.5' \times 20.5'$	0.62	16 / 143 <sup>a</sup> d	1 hr / 1 d
Nardiello et al. (2015)	Asiago 67/92 cm Schmidt (OAPD)	$\approx 58' \times 38'$	0.86	$\geq 10$ d	3 min
Libralato et al. (2016)	Kepler (K2)	$115^\circ$	3.98	$\approx 31$ d	1 min / 29 min <sup>b</sup>
Soares-Furtado et al. (2020)	Kepler (K2)	$115^\circ$	3.98	$\approx 31$ d	29 min
This Work	Samuel Oschin Telescope (Palomar Observatory; ZTF)	$47^\circ$	1.00	several yrs	1 - 2.5 d

**Notes.** <sup>(a)</sup> High-frequency (once per hr for 5–6 hrs per night) time-series photometric observations were taken over 16 nights and complemented with low-frequency (once per night) observations taken over 143 nights. <sup>(b)</sup> *Kepler* exposures are combined on board to create short-cadence timeseries (nine co-added exposures) or long-cadence timeseries (270 co-added exposures). See Koch et al. (2010) and references therein for a detailed description of the *Kepler* design.

rotators in M35. By matching our catalog with that of Meibom et al. (2009), we obtained periods for 109 stars in our sample. A similar choice was made by Jeffries et al. (2021), who chose the periods published in Meibom et al. (2009) instead of the ones derived by Libralato et al. (2016) when both were available.

For those stars lacking periods in Meibom et al. (2009), we turned to the ones derived from K2 light curves. From Soares-Furtado et al. (2020), we selected periods for the 31 stars classified as rotating with no blending. In addition, we adopted the period published for one star classified as indeterminate variable.

We have taken advantage of the periods not flagged as possible blends in Libralato et al. (2016, flags 0 and 30) to obtain rotation periods for 39 stars not included in Soares-Furtado et al. (2020). In addition, we recovered one period from Libralato et al. (2016) for a star classified in Soares-Furtado et al. (2020) as an eclipsing binary.

Finally, we obtained rotation periods for six stars from Nardiello et al. (2015). Two have no counterparts in Meibom et al. (2009), Libralato et al. (2016), Soares-Furtado et al. (2020); one has an invalid period ( $Prot = -99.0$ ) in Libralato et al. (2016); and three are considered blends in Soares-Furtado et al. (2020). As Nardiello et al. (2015) analysed light curves taken by an instrument whose plate scale is much smaller than *Kepler*'s, we considered that these light curves were unlikely to be affected by blending and that these periods are reliable.

#### 4.2. New rotational periods from ZTF light curves

ZTF has observed M35 regularly since 2018 March 25. Following Curtis et al. (2020), we extracted differential photometry from the archival ZTF imaging using nearby reference stars in the field. Although the resulting light curves are much sparser and more irregularly sampled than those from dedicated photometric surveys, they can still yield reliable period measurements. Our goal in analyzing these light curves was twofold: ZTF-derived periods can provide confirmation of periods in the literature, and ZTF light curves generally cover much longer timespans than those of other photometric surveys, and can therefore be used to measure periods for slower rotators in M35.

We inspected the light curves for each available season, computed Lomb–Scargle periodograms, and then recorded the period if it was significant and produced a convincing phase-folded

light curve. In this manner, we measured periods for nine stars lacking periods in the literature, for one star classified as rotating with blending in Soares-Furtado et al. (2020), and for 37 stars with valid periods in the aforementioned surveys. For stars with periods in the literature, the average agreement between our measurements and the existing values is  $<1\%$ , and the differences are  $\leq 10\%$ . We have chosen the periods derived from ZTF light curves for these 47 members of M35.

#### 4.3. Final sample of M35 members with Li measurements and rotation periods

Combining the periods we derived and those collected from the literature, we obtained rotation periods for 197 of the 251 members of M35 observed with Hydra. Table 6 provides the periods for these 197 stars.

## 5. Analysis

### 5.1. Deriving effective temperatures and luminosities

We generated the SED of each star in our sample with VOSA (version 7.5; Bayo et al. 2008) using the photometry in Table 7, which was taken from Bouy et al. (2015) and Barrado y Navascués et al. (2001b). We also used VOSA to cross-match our sample with a number of catalogs, obtaining photometry in the PAN-STARRS/PS1 filters, Misc/APASS filters, WISE filters, INT/IPHAS filters, and Palomar/ZTF filters. Following an approach similar to that taken by Jeffries et al. (2021), we assumed a distance of  $885 \pm 80$  pc for all the stars and a visual extinction in their direction of  $A_V = 0.62$ .

The dereddened SEDs obtained in this manner were compared with Kurucz model atmospheres (Castelli et al. 1997; Castelli & Kurucz 2003), assuming  $\log g = 4.5$  and a solar metallicity, to determine the luminosity and effective temperature that best fit each SED using a  $\chi$ -squared minimisation method. Figure 2 shows the Hertzsprung–Russell diagram (HRD) built with the astrophysical parameters obtained, which are listed in Table 9. As we could not obtain a reliable fit in VOSA for star number 7028, we excluded it from our study and focused on the remaining 250 cluster members.

**Table 6.** Rotation periods taken from the literature or derived from ZTF light curves for 197 M35 members. M09 is Meibom et al. (2009), SF20 is Soares-Furtado et al. (2020), N15 is Nardiello et al. (2015), and L16 is Libralato et al. (2016). This table is only partially presented. Its complete version is available electronically.

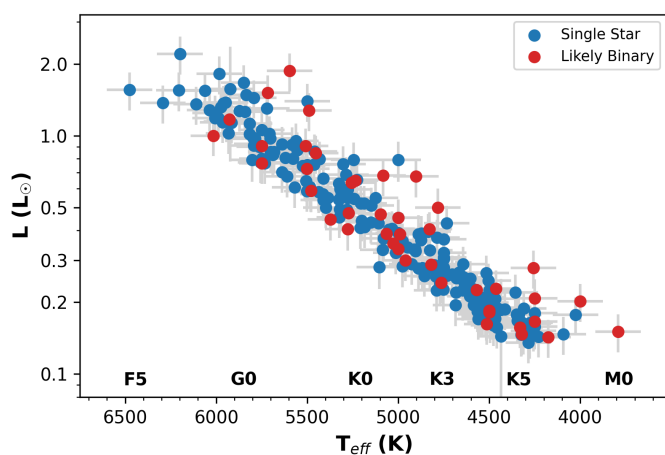
ID	Prot (d) M09	Prot (d) SF20	Class <sup>a</sup> SF20	Subclass <sup>b</sup> SF20	Blend <sup>c</sup> SF20	Prot (d) L16	Flag <sup>d</sup> L16	Prot (d) N15	Type <sup>e</sup> N15	Prot (d) ZTF	Final Prot (d)
5483	–	–	–	–	–	0.48	1	0.48	Rot	0.48	0.48
7118	1.10	1.11	Rotating	RotVar	0	1.11	1	1.10	Rot	1.11	1.11
5356	–	–	–	–	–	–	–	–	–	7.01	7.01
5459	7.30	–	–	–	–	7.19	1	–	–	–	7.30
7076	–	2.44	Rotating	RotVar	0	–	–	–	–	–	2.44
...	...	...	...	...	...	...	...	...	...	...	...

**Notes.** <sup>(a)</sup> *Rotating* accounts for rotational variables, *Pulsating* for pulsating variables, *EB* for eclipsing binaries, and *Misc* for indeterminate variables. <sup>(b)</sup> *RotVar* accounts for rotational variables of indeterminate type, *GDor* for  $\gamma$  Doradus pulsators, *EB* for eclipsing binaries, and *Misc* for indeterminate variables. <sup>(c)</sup> 0 = identified primary variable, 1 = ambiguous blend. <sup>(d)</sup> 0 = high probability that it is a blend; 1 = candidate variable; 2 = difficult to classify; 30 = difficult to classify star that, by comparison with the literature, could be a possible blend; 31 = difficult to classify star for which a correspondence in the literature was found. <sup>(e)</sup> *Rot* are rotating stars, *EB* eclipsing binaries, *Long-Period* long-period variables, and *delta Sct*  $\delta$  Scuti stars.

**Table 7.** Photometry uploaded to VOSA for the 251 members of M35 in our sample. This table is only partially presented. Its complete version is available electronically.

ID	V <sup>a</sup>	Ic <sup>b</sup>	g <sup>c</sup>	r <sup>c</sup>	i <sup>c</sup>	z <sup>c</sup>	J <sup>d</sup>	H <sup>d</sup>	Ks <sup>d</sup>
5408	17.258	15.825	–	16.91±0.05	16.50±0.03	16.13±0.03	14.81±0.06	14.17±0.06	13.98±0.04
5087	14.652	13.743	15.07±0.05	14.58±0.13	14.15±0.11	14.08±0.03	13.15±0.02	12.82±0.02	12.68±0.02
5382	17.136	15.661	–	16.51±0.03	16.21±0.03	15.90±0.03	14.66±0.06	14.11±0.06	13.97±0.05
5194	15.756	14.607	16.29±0.05	15.41±0.05	15.10±0.03	14.88±0.03	13.76±0.03	13.27±0.03	13.18±0.03
7034	–	–	18.45±0.05	17.16±0.05	16.69±0.03	16.40±0.03	15.11±0.06	14.53±0.06	14.40±0.07
...	...	...	...	...	...	...	...	...	...

**Notes.** <sup>(a)</sup> Johnson V band magnitude taken from Barrado y Navascués et al. (2001b). <sup>(b)</sup> Cousins I band magnitude taken from Barrado y Navascués et al. (2001b). <sup>(c)</sup> SDSS magnitudes taken from Bouy et al. (2015). <sup>(d)</sup> 2MASS magnitudes taken from Bouy et al. (2015).

**Fig. 2.** Positions in the HRD for the 250 members of M35 in our sample whose effective temperatures and bolometric luminosities were determined by SED fitting with VOSA. Red circles are binary systems, while blue circles are single stars.

## 5.2. Measuring equivalent widths and abundances

We used the iSpec software to combine RV-corrected versions of the spectra collected during our 1999 and 2001 campaigns. This allowed us to obtain a single spectrum for each of the stars observed during each campaign with a signal-to-noise ratio (SNR) >300.

We also used iSpec to develop the pipeline to derive the EqW(Li) and Li abundance for each star. First, we used the

SPECTRUM radiative transfer code described in Gray & Corbally (1994), the MARCS model atmospheres (Gustafsson et al. 2008), and the *Gaia*–ESO survey line list (Heiter et al. 2021) to generate, for each star, a synthetic  $R = 20,000$  spectrum with solar metallicity,  $\log g = 4.5$ , and the effective temperature returned by VOSA. This process was repeated several times while modifying the rotational velocity until we found the  $v \sin i$  that best fits the science spectrum.

Second, we determined the iron abundance for each star using 40 Fe lines between 645 nm and 680 nm together with the aforementioned stellar parameters. Once the rotational velocity and the Fe abundance have been determined, these parameters, together with the radiative transfer code, model atmospheres, and line list previously mentioned, were used to derive the EW of the Li doublet at 670.78 nm as well as the local thermodynamic equilibrium (LTE) Li abundance. Both quantities were measured three times for each star while modifying slightly the continuum value, and their uncertainties were calculated as the standard deviation of those measurements.

However, as the resolution of the spectra is not high enough to separate the Li doublet at 670.78 nm and the Fe I line at 670.75 nm, both features are blended (see Figure 3, where a small region around the Li doublet is shown for four K stars). To remove the contribution of this iron line, we have tried two different approaches.

First, we built a synthetic spectrum employing a modified version of the *Gaia*–ESO line list where all the Li lines had been removed. The SNR estimated for the science spectrum was used to add errors to the synthetic one for each star. The EW corresponding to the Fe I line at 670.75 nm was then subtracted from the EW of the blend, resulting in a measurement of the EW of

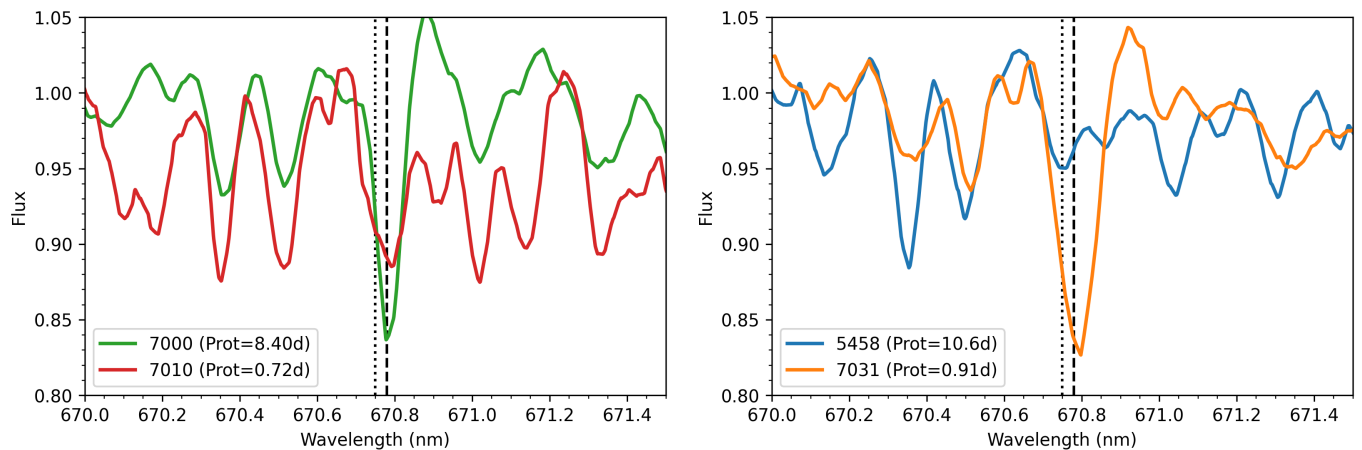


**Fig. 3.** Blended feature around 670.78 nm for four K stars. *Left*— Small region of the spectrum for two mid K stars with different rotation periods. *Right*— Small region of the spectrum for two late K stars with different rotation periods. In both panels, the dashed black line shows the position of the Li doublet at 670.78 nm, while the dotted black line indicates the position of the Fe I line at 670.75 nm. Both features are blended independently of the spectral type and the rotation period of the star.

the Li doublet. The uncertainty in  $EW(\text{Li})$  width was derived from the quadratic sum of the uncertainty in the blend and the uncertainty in the  $EW$  of the Fe I line.

Second, we followed the approach of [Arancibia-Silva et al. \(2020\)](#): we derived (B-V) colours for our stars from the dereddened *Gaia* (BP - RP) colours, and we applied the empirical relation derived in [Soderblom et al. \(1993\)](#). To obtain intrinsic (B-V) colours for the targets observed in these campaigns we linearly interpolated through the [Pecaut & Mamajek \(2013\)](#)  $(B-V)_0 - (BP-RP)_0$  relationship. Finally, we calculated the contribution of the the Fe I line at 670.75 nm as  $EW(\text{Fe}) = 20 (B-V)_0 - 3 \text{ m}\text{\AA}$ .

The left panel on Figure 4 shows the comparison between the Li EWs obtained by these two approaches. The median of the differences is around 10 mÅ, as indicated by the dotted black line, and the spread around this value is small.

The right panel of Figure 4 shows the comparison between the Li EWs published in [Jeffries et al. \(2021\)](#) and the values obtained by employing the [Soderblom et al. \(1993\)](#) relation. [Jeffries et al. \(2021\)](#) measured the Li EWs by comparing the science spectra with synthetic spectra without Li generated with the MOOG software ([Snedden et al. 2012](#)) and solar-metallicity Kurucz model atmospheres ([Kurucz 1992](#)). The median of the differences is around 20 mÅ in this case, as indicated by the dotted black line, and the spread around this line is broader than the one shown in the left panel. Since the equivalent widths shown in the left panel have been derived from the same spectra, unlike the ones shown in the right panel, a broader spread in the latter is not surprising.

In Figure 5, we plot the iron equivalent widths obtained from the [Soderblom et al. \(1993\)](#) empirical relation and those measured in the synthetic spectra, confirming a  $\approx 5 \text{ m}\text{\AA}$  difference between G0 and early K spectral types, which gets larger than 10 mÅ for stars cooler than  $(BP-RP)_0 = 1.2$ . Since [Soderblom et al. \(1993\)](#) derived their relation from the spectra of inactive, old field stars with spectral types earlier than K3, a large difference for cooler dwarfs is not surprising. The smaller differences observed in hotter stars could have a methodological or an intrinsic origin. It is possible that the empirical relation proposed by [Soderblom et al. \(1993\)](#) takes into account fainter contributions from other elements different from iron that are not included in the synthetic spectra. However, given the completeness of the

line list employed to generate the synthetic spectra, this explanation is unlikely. An alternative explanation could be that the [Soderblom et al. \(1993\)](#) relation is useful for solar metallicity clusters, like the Pleiades, but overestimates the contribution of the Fe I line at 670.75 nm to the blended feature for subsolar metallicity clusters, such as M35. Consequently, we used the Li EWs obtained using synthetic spectra to remove the contribution of the Fe I line for our analysis.

Finally, we estimated the departures from LTE for the Li abundances derived from the non-LTE calculations published in [Lind et al. \(2009\)](#). To do so, we split our stars in bins of effective temperature and linearly interpolated through [Lind et al. \(2009\)](#) non-LTE correction– $A(\text{Li})$  LTE relationship.<sup>4</sup>

Table 8 gives the derived Li EWs, the Fe EWs obtained with the two methods described above, as well as the LTE and non-LTE Li abundances for our stars.

## 6. Results

### 6.1. The metallicity of M35

Previous WIYN/Hydra spectroscopic studies of Li in M35 quoted different values for its metallicity. [Barrado y Navascués et al. \(2001a\)](#) derived  $[\text{Fe}/\text{H}] = -0.21 \pm 0.10$  by measuring Fe EWs for a set of single G members of the cluster, whereas [Steinhauer & Deliyannis \(2004\)](#) set  $[\text{Fe}/\text{H}] = -0.143 \pm 0.014$  when studying Li depletion in the cluster’s F dwarfs. On the other hand, [Anthony-Twarog et al. \(2018\)](#) measured the EW of the Ca I line at 671.77 nm and obtained results compatible with solar metallicity. [Jeffries et al. \(2021\)](#) assumed a solar metallicity for their analysis, but discussed the impact a lower metallicity could have on their results.

As discussed in §5.2, we used 40 iron lines to derive the abundance of this element for each of the M35 members observed in 1999 December and 2001 February. This list includes 38 Fe I transitions and two Fe II transitions. The results obtained for those single stars with the highest probability of belonging to M35 were employed to derive our own value for the metallicity for this cluster.

<sup>4</sup> We selected the rows in table 2 of [Lind et al. \(2009\)](#) for a solar metallicity and microturbulence  $\xi_t = 1.0 \text{ km s}^{-1}$ .

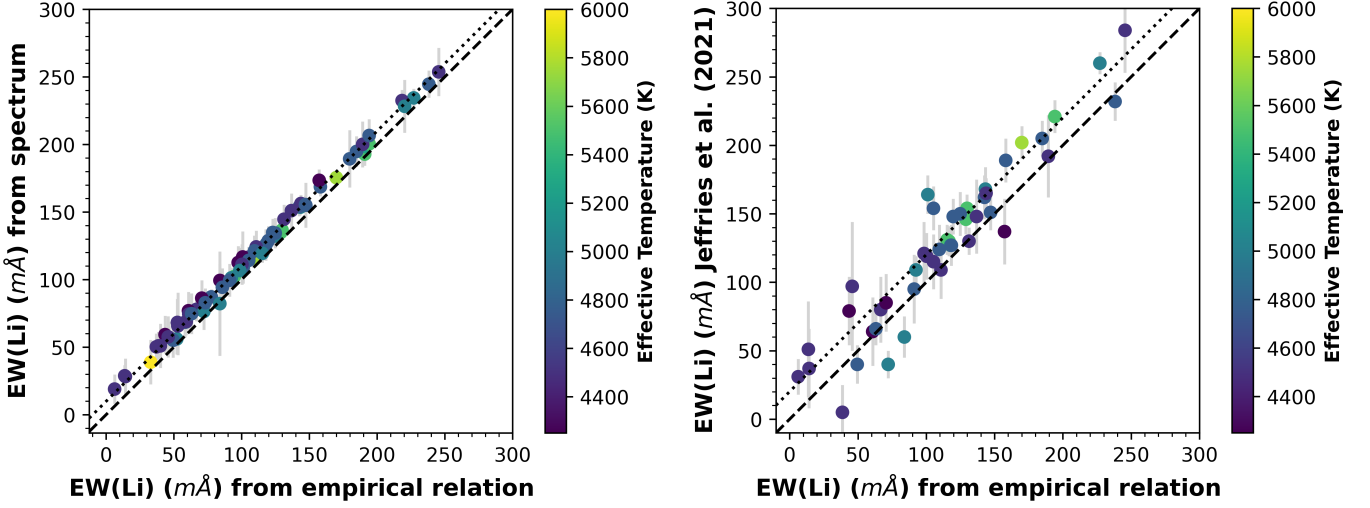


**Fig. 4.** Comparisons between the Li EWs derived by applying the empirical relation published in Soderblom et al. (1993) to the M35 spectra collected in 1999 December and 2001 February (x axes) and the EWs obtained by other methods for the same objects (y axes). *Left*—Comparison to Li EWs obtained using synthetic spectra without Li generated with the SPECTRUM code and MARCS model atmospheres. *Right*—Comparison to Li EWs published in Jeffries et al. (2021). In both panels, the dashed black line shows the one-to-one correspondence, while the dotted line indicates the median of the differences. The colour of each symbol indicates the effective temperature derived for the star. In both cases, the EWs indicated on the y axes are, on average, larger than the ones shown on the x axes.

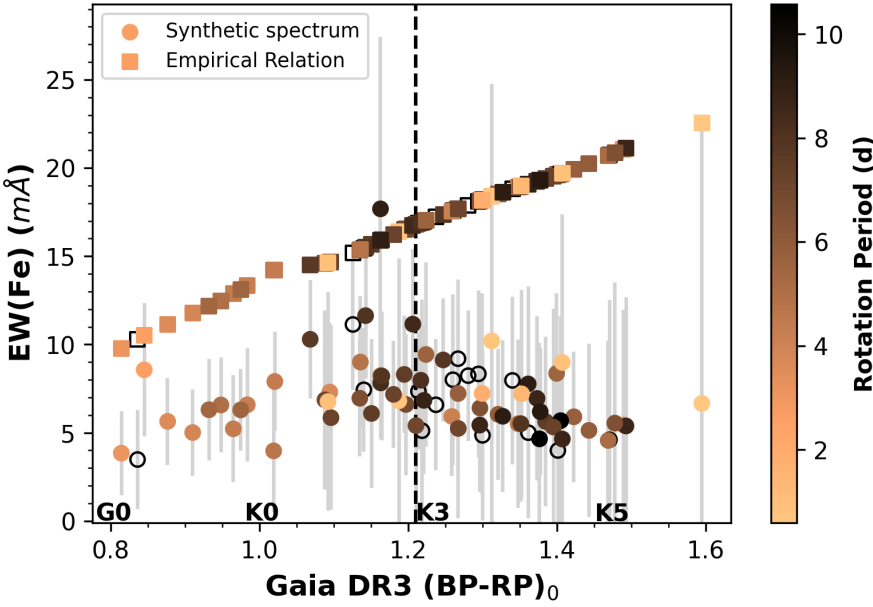


**Fig. 5.** EWs measured for the Fe I line at 670.75 nm in the synthetic spectra and those derived from the empirical law proposed by Soderblom et al. (1993). *Gaia* colours have been dereddened using  $E(BP - RP) = 0.415 A_V$ , following Curtis et al. (2020). The colour of each symbol indicates the rotation period of the star. The Soderblom et al. (1993) relation was derived from spectra of stars on the left side of the vertical dashed line. The EWs obtained for stars on the right side of the line are therefore obtained by extrapolating that relation to a cooler range of temperatures.

**Table 8.** Blended Li and Fe EWs, Fe EWs, Li EWs, and Li LTE and non-LTE abundances for the 110 members of M35 observed in 1999 December and 2001 February. This table is only partially presented. Its complete version is available electronically.

ID	$EW(Li+Fe)$ (mÅ)	$EW(Fe)^a$ (mÅ)	$EW(Fe)^b$ (mÅ)	$EW(Li)^a$ (mÅ)	$A(Li)_{LTE}$	$A(Li)_{NLTE}$
5088	119.2±6.5	3.5±2.8	10.3	115.7±7.1	2.88±0.04	2.85
5103	201.4±7.6	8.6±3.8	10.5	192.9±8.5	2.98±0.03	2.92
5139	127.1±5.2	5.0±2.5	11.8	122.0±5.7	2.66±0.03	2.68
5148	181.1±4.7	5.6±2.5	11.1	175.5±5.3	3.22±0.03	3.06
5183	107.6±5.1	5.2±3.0	12.9	102.3±5.9	2.57±0.03	2.59
5295	≤14.3 <sup>c</sup>	–	–	–	–	–
...	...	...	...	...	...	...

**Notes.** <sup>(a)</sup> Value obtained from the synthetic spectrum without Li. <sup>(b)</sup> Value obtained from the empirical relation of Soderblom et al. (1993). <sup>(c)</sup> Upper limit. Li abundances and Fe EWs are not provided for these cases.

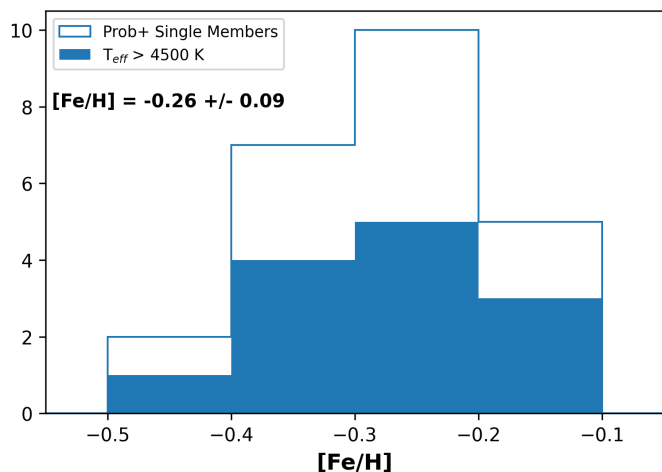


**Fig. 6.** Metallicities obtained for the single stars observed in 1999 December and 2001 February that have the highest probability of belonging to M35 (*Prob+* members). The unfilled histogram represents the distribution of metallicities obtained for all of them, whereas the filled histogram only includes the hottest stars in this sample. We used the values corresponding to the hottest ones to derive a metallicity of  $[\text{Fe}/\text{H}] = -0.26 \pm 0.09$  for M35.

As shown in Figure 6, our results clearly point to a subsolar metallicity for M35. We have only considered the hottest stars ( $T_{\text{eff}} > 4500$  K) in the set previously described, obtaining an average metallicity of  $[\text{Fe}/\text{H}] = -0.26 \pm 0.09$ , where the standard deviation of the values has been used to indicate the uncertainty. This result is fully consistent with the values published in Barrado y Navascués et al. (2001a) and Steinhauer & Deliyannis (2004).

## 6.2. The Li-rotation connection in M35

Figure 7 is a color–period diagram in which we indicate the relative Li abundances of the stars in M35; the top panel includes all of the cluster members, whereas in the bottom panel we have removed candidate and known binary systems. Table 9 includes the stellar parameters, rotation periods, and Li EWs for these stars. The most striking result is that M35 fast rotators of G and K spectral types are Li-rich compared with slow rotators of similar effective temperature. This result is consistent with the pattern described in Barrado y Navascués et al. (2001a), Anthony-Twarog et al. (2018) and Jeffries et al. (2021) for the M35 open cluster as well as with the trend found for other stellar associations (see Bouvier 2020, and references therein).

Few studies have addressed the influence of a stellar companion on the Li abundance. Martín et al. (2002) studied the abundance of this element in wide binaries with solar-type twin components, finding large differences between the components for a significant part of the sample. Barrado y Navascués & Stauffer (1996) demonstrated that tidally locked binaries in the Hyades open cluster are richer in Li in comparison with single stars. The purpose of the present article is not to characterize Li in binary systems, but it is worth highlighting that the difference in Li EWs between fast and slow G and K rotators is more evident in the bottom panel of Figure 7, where multiple systems are not included.

The M0 fast rotator shown in the top panel deserves special attention. This star is a spectroscopic binary with identification number 5517 which was observed in 1999 December. We have

measured  $\text{EW}(\text{Li}) \leq 24.1$  mÅ for this object, which is a value very similar to the EWs derived by Bouvier et al. (2018) and Barrado et al. (2016) for Pleiades members of similar spectral type and rotation period.

Four outliers, which are circled in the bottom panel of Figure 7, do not follow the trend described above. The hottest, whose Li EW has been taken from Anthony-Twarog et al. (2018), has the identification number 5181 (46015 in Anthony-Twarog et al. 2018). Its rotation period has been taken from Meibom et al. (2009), but very similar periods are considered ambiguous blends in Soares-Furtado et al. (2020) and Libralato et al. (2016), so the rotation period of this source may be different from the one we have assigned it in Table 6. This source is also considered as an outlier in Anthony-Twarog et al. (2018) (see section 4 of that work).

Two fast rotators, 7049 and 7053, observed in 1999 December and 2001 February have Li EWs that are surprisingly low. The membership of star 7049 is doubtful since both the probability provided by Clusterix 2.0 and the radial velocity measured for this star indicate it does not belong to M35. Consequently, the membership probability assigned in Bouy et al. (2015) to this source may be wrong. By contrast, star 7053 has the highest probability of belonging to M35. However, only Meibom et al. (2009) provides rotation period for this star, and comparing their result with those of others is therefore not possible. Both sources were studied by Jeffries et al. (2021), who obtained Li EWs compatible with the ones shown in Table 8.

Finally, the equivalent width of the remaining outlier, star 5290, has been taken from Jeffries et al. (2021). In contrast to the other sources, there is no reason to think that the rotation period assigned to this star is mistaken, nor that it is not member of M35. Follow-up observations of this star are needed to understand the reason why it is Li-poor in comparison with the other fast rotators. In any case, it is clear that the aforementioned connection between Li and rotation holds.

## 6.3. Comparison with other clusters

We have included in Figure 8 and Figure 9 the single stars studied by Jeffries et al. (2021) that do not have counterparts in our sample (top panels), as well as equivalent data for the Pleiades for comparison (bottom panels). Galindo-Guil et al. (2022) recently provided a robust value of  $127.4^{+6.3}_{-10}$  Myr for the age of the Pleiades by employing the Li depletion boundary technique described in Soderblom et al. (2014), Rebolo et al. (1992, 1996), and Stauffer et al. (1998, 1999). Although the age of M35 is affected by a much higher uncertainty, given the values provided by Jeffries et al. (2021) and Anthony-Twarog et al. (2018) ( $140 \pm 15$  Myr and  $150 \pm 25$  Myr, respectively) both clusters could be coeval. In fact, Abdelaziz et al. (2022) obtained an age of 126 Myr for M35 by using the Padova isochrones of Marigo et al. (2017) to fit the turnoff point in several color–magnitude diagrams. We assumed that the age of M35 is between 125 Myr and 175 Myr, the latter being the value provided by Barrado y Navascués et al. (2001a).

The metallicity of the Pleiades is very close to solar. Boesgaard & Friel (1990) derived  $[\text{Fe}/\text{H}] = -0.034 \pm 0.024$  from a sample of F dwarfs whereas Gebran & Monier (2008) obtained  $[\text{Fe}/\text{H}] = 0.06 \pm 0.02$ . Given the metallicity derived for M35 by Barrado y Navascués et al. (2001a), Steinhauer & Deliyannis (2004), and this work, M35 is metal poor in comparison with the Pleiades. Despite this difference in metal content and a possible difference in age, the trends shown in Figures 8 and 9 for M35 and the Pleiades are very similar. In both cases, fast rota-

**Table 9.** Rotation period, Li EW, effective temperature, luminosity, membership class and binary status for 250 M35 members. This table is only partially presented. Its complete version is available electronically.

ID	Membership Class	Binary <sup>a</sup>	$T_{eff}$ (K)	$L$ ( $L_{\odot}$ )	$EW(Li)$ ( $m\text{\AA}$ )	$EW(Li)^b$ Source	Prot <sup>c</sup> (d)	Prot <sup>d</sup> Source
5408	Poss+	0	4500±125	0.21±0.04	291	B01	0.74	M09
5087	Poss+	0	6000±125	1.57±0.79	101.7	AT18	2.20	SF20
5382	Prob	0	4750±125	0.26±0.05	187	Je21	3.08	M09
5194	Poss	1	5000±125	0.68±0.12	153.6	This Work	4.70	M09
7034	Prob	0	4500±125	0.16±0.03	≤ 29.9	This Work	9.71	M09
5107	Poss+	0	6000±125	1.38±0.26	94	B01	2.51	This Work
...	...	...	...	...	...	...	...	...

**Notes.** <sup>(a)</sup> 1 = likely binary, 0 = single star. <sup>(b)</sup> B01 is [Barrado y Navascués et al. \(2001a\)](#), AT18 is [Anthony-Twarog et al. \(2018\)](#), and Je21 is [Jeffries et al. \(2021\)](#). <sup>(c)</sup> -99 = No rotation period available for this source. <sup>(d)</sup> M09 is [Meibom et al. \(2009\)](#), SF20 is [Soares-Furtado et al. \(2020\)](#), N15 is [Nardiello et al. \(2015\)](#), and L16 is [Libralato et al. \(2016\)](#).

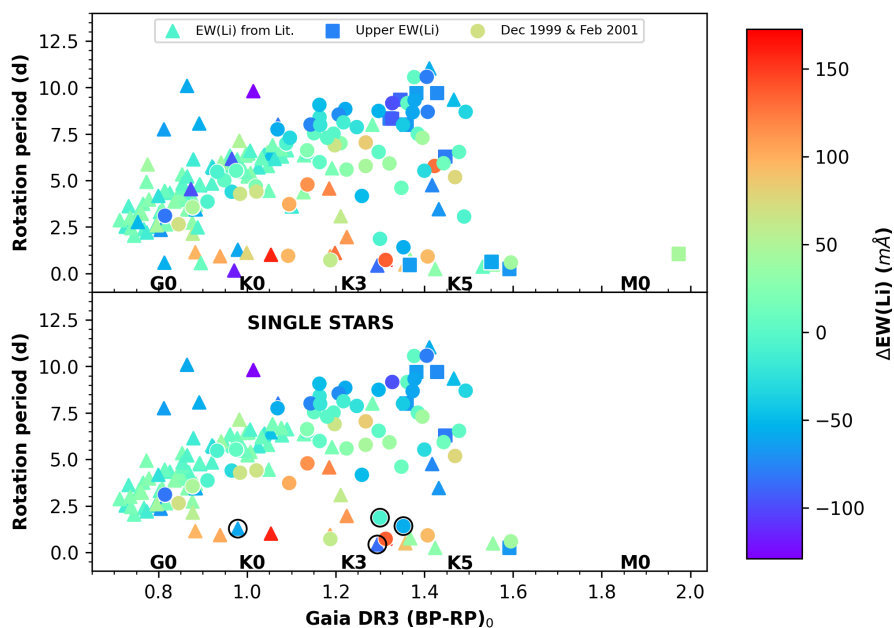


**Fig. 7.** Distribution of rotation periods for the M35 members in our sample. The colour of each symbol indicates the deviation of the  $EW(Li)$  obtained for that star from a third order polynomial fit to  $EW(Li)$  vs.  $(BP - RP)_0$ . Circles indicate the M35 members observed in 1999 December and 2001 February whose Li EWs have been derived as discussed in section 5.2, while triangles are those M35 members whose Li EWs have been taken from [Barrado y Navascués et al. \(2001a\)](#), [Anthony-Twarog et al. \(2018\)](#), or [Jeffries et al. \(2021\)](#). Squares denote those stars observed in 1999 December and 2001 February for which we could only derive upper limits for the Li EWs. *Top*—Our complete set of M35 members with rotation periods. *Bottom*—Only those sources classified as single stars are shown. The four outliers that do not follow the general trend are circled in black.

tors are richer in Li than slow rotators of the same spectral type. This connection is more evident for K stars than for G stars as the spread is larger in that range of effective temperatures.

We also compared our results for M35 to those for M34. [Ianna & Schlemmer \(1993\)](#) estimated an age of 250 Myr for M34 through isochrone fitting, whereas [Meynet et al. \(1993\)](#) derived an age of 178 Myr for this cluster employing the same technique. [Schuler et al. \(2003\)](#) derived  $[Fe/H] = 0.07 \pm 0.04$  from high resolution spectra of five G-K dwarf members of the cluster. Since M34 is older than M35 and has solar metallicity, as do the Pleiades, we have compared our sample of M35 single dwarfs of G-K spectral type with the one presented in [Gondoin \(2014\)](#) for M34 (Figure 10). Although the similarities between both distributions are more evident in Figure 9, as the Pleiades sample is more similar in size to that for M35, a similar trend can be observed for M34 K dwarfs: the fast rotators are richer in Li than the slow ones.

To statistically compare the Li measurements collected for the three clusters, we have performed Kolmogorov-Smirnov tests between them ([Hodges 1958](#)). The purpose of this test is to verify whether two samples (in this case, the Li EWs collected) have been taken from the same continuous distribution. We have only considered single stars with rotation periods  $>2$  d (to avoid

contamination from rapid rotators) and absolute Li EWs (not upper values). Figure 11 shows the empirical distribution functions obtained for each of the 1000 tests performed between the Li EWs sample corresponding to M35 and the samples corresponding to the Pleiades and M34. The median of the p-values obtained in both cases (shown in the panels of the figure) do not allow us to rule out the possibility that the three samples come from the same continuous distribution, implying a clear similarity between them. On the other hand, the median of the p-values obtained when we compared the Pleiades sample and the M34 sample in the same way is higher, indicating a larger difference between the Li distributions of these two clusters.

## 7. Summary and conclusions

We collected a sample of 396 G and K dwarfs observed with the Hydra spectrograph of the 3.5-m telescope located at WYIN Observatory. We analysed the photometry, proper motions, and radial velocities of these sources, identifying 251 members of the M35 open cluster, 209 of which are single stars. In addition, we obtained rotation periods for 47 of these sources from ZTF light curves and we took advantage of previous photometric surveys, obtaining rotation periods for 197 M35 members in total.

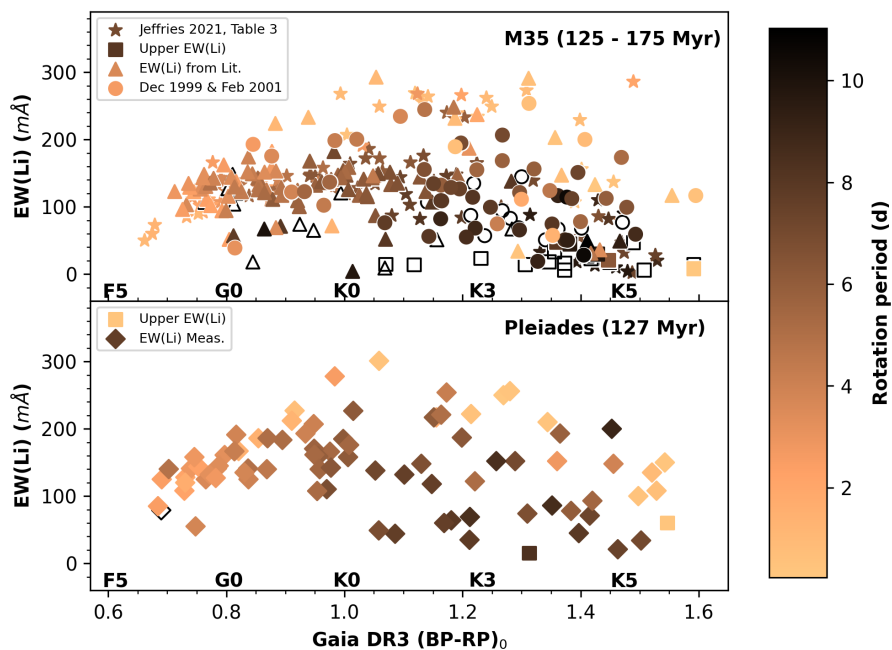


**Fig. 8.** Li EWs vs. *Gaia* colours for single members of M35 and the Pleiades. The symbols are colour-coded by the rotation period of the star. The empty symbols are M35 members without a measure rotation period. *Top*—M35 single stars. Circles, triangles, and squares have the same meaning as in Figure 7. We use star symbols to represent the single stars analysed by Jeffries et al. (2021) that do not have counterparts in our sample. *Bottom*—Pleiades single stars taken from Barrado et al. (2016) and Bouvier et al. (2018). Note that we have chosen the Li EWs and rotation periods published in Bouvier et al. (2018) for all of the stars that are included in both studies. We have only plotted those Pleiades members whose *Gaia* colours are within the range covered by the M35 sample shown in the top panel. *Gaia* colours have been dereddened following Curtis et al. (2020) with  $A_V = 0.12$ .

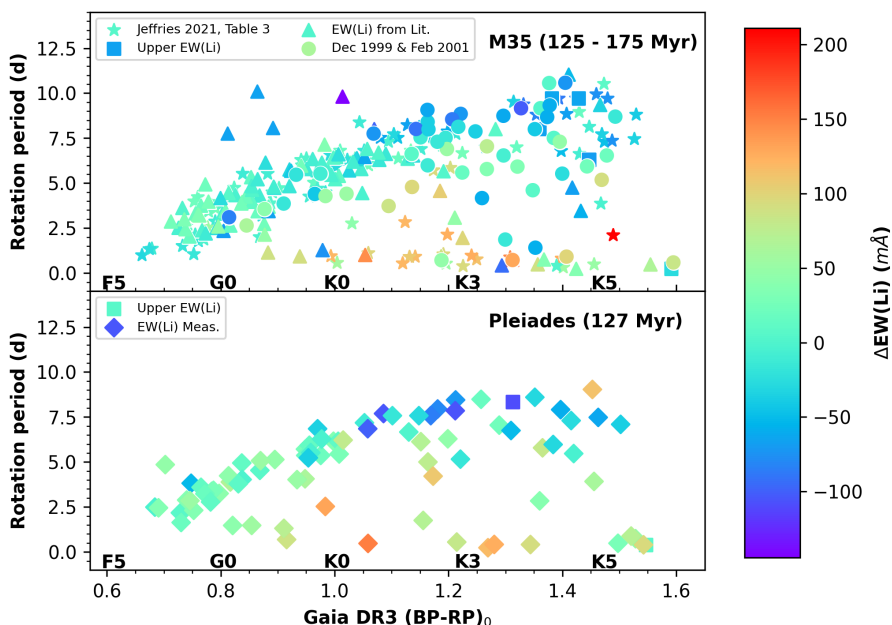


**Fig. 9.** Rotation periods vs. *Gaia* colours for single members of M35 and the Pleiades. The colour of each symbol indicates the deviation of EW(Li) from a third-order polynomial fit to EW(Li) vs.  $(BP - RP)_0$  for the M35 sample shown in the upper panel. *Top*—M35 single stars. Circles, triangles, and squares have the same meaning as in Figure 7 whereas stars account for the M35 single sources analysed in Jeffries et al. (2021) which do not have counterpart in our sample. *Bottom*—Pleiades single stars taken from Barrado et al. (2016) and Bouvier et al. (2018). Note that we have chosen the Li EWs and rotation periods published in Bouvier et al. (2018) for all the sources which have counterpart in both studies. We have only plotted those Pleiades members whose *Gaia* colours are within the range covered by the M35 sample shown on the top panel. *Gaia* colours have been dereddened following Curtis et al. (2020) with  $A_V = 0.12$ .

We analysed the spectra collected for 110 out of 251 M35 members, deriving iron abundances, Li EWs and non-LTE Li abundances for them. From the iron abundances obtained for the most probable single members with effective temperatures higher than 4500 K we derived a metallicity of  $[Fe/H] = -0.26 \pm 0.09$  for M35. In addition, we found that the empirical law proposed in Soderblom et al. (1993) for the Pleiades overestimates the equivalent width of the Fe I line at 670.75 nm in 5 - 15 mÅ for the range of effective temperatures analysed. As a result, we conclude that the Soderblom et al. (1993) empirical relation is not recommended for subsolar metallicity clusters.

We combined the Li EWs that we measured with data collected from previous studies, obtaining rotation periods and Li EWs for 257 single members of M35. The Li-rotation connection found for this sample follows the trend observed in similar studies of M35 as well as with the trend found for other stellar

associations: fast rotators are richer in Li than slower rotators of the same effective temperature.

Finally, we compared our sample with that for two open clusters with solar metallicity: the Pleiades, which is slightly younger than M35, and M34, which is slightly older. From the Kolmogorov-Smirnov tests performed, no significant statistical difference was observed between the Li EWs distribution for M35 and those for the other clusters. However, a larger difference is found between the M34 sample and the Pleiades one. As a result, we conclude that a 0.2 - 0.3 dex difference in metallicity does not have an observable impact on the Li distributions of open clusters with ages between 100 and 250 Myr. The statistical analysis carried out points to age as the parameter that most influences the evolution of Li in open clusters.

*Acknowledgements.* This research has been funded by grant No. PID2019-107061GB-C61 by the Spanish Ministry of Science and Innovation/State Agency

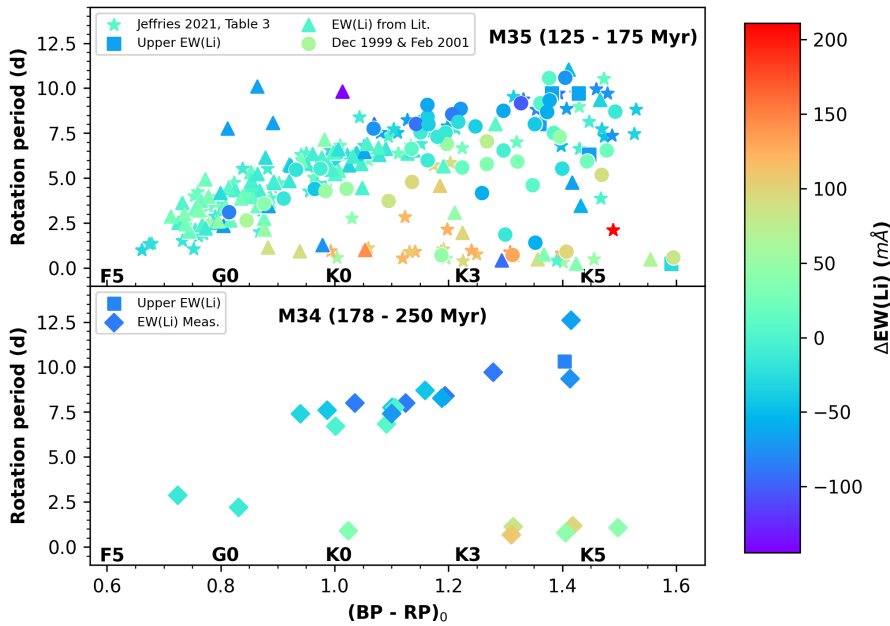


**Fig. 10.** Rotation periods vs. *Gaia* colours for single members of M35 and M34. The colour of each symbol indicates the deviation of EW(Li) from a third order polynomial fitted to EW(Li) vs  $(BP - RP)_0$  for the M35 sample shown in the upper plot. *Top*—M35 single stars. Circles, triangles, squares, and stars have the same meaning as in Figure 9. *Bottom*—M34 single stars from Gondoin (2014). *Gaia* colours have been dereddened following Curtis et al. (2020) with  $A_V = 0.217$ .

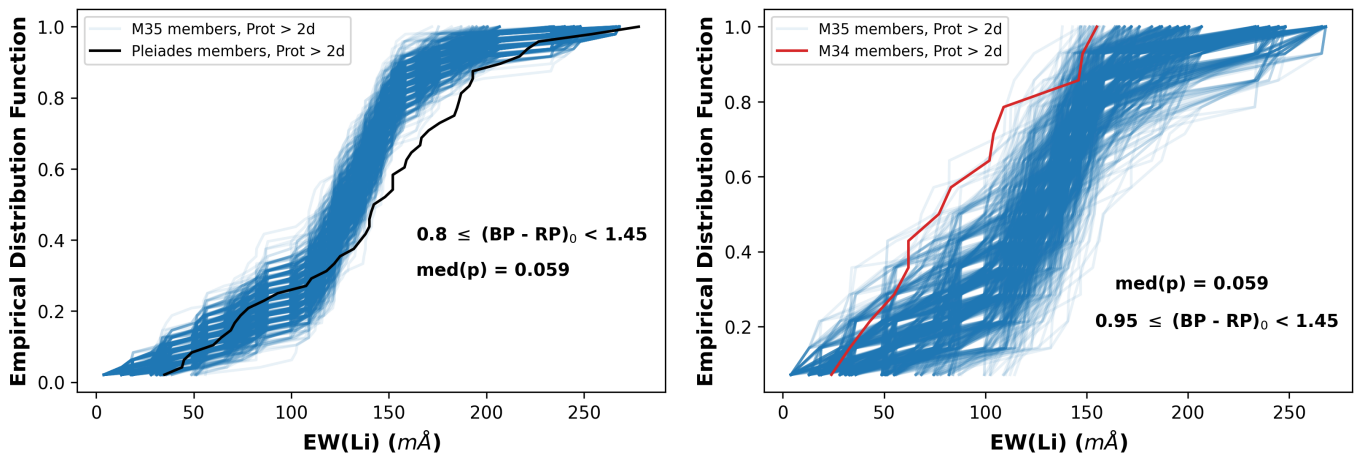


**Fig. 11.** Empirical distribution functions obtained from 1000 Kolmogorov-Smirnov tests performed between the Li EWs sample corresponding to M35 and those of other clusters. *Left*—Pleiades Li EWs sample (see Figures 8 and 9). For each test we have randomly picked 48 Li EWs from the M35 sample (blue), that is, the size of the Pleiades sample, and compared them with the Pleiades sample (black). *Right*—M34 Li EWs sample (see Figure 10). For each test we have randomly picked 14 Li EWs from the M35 sample, and compared them with the latter (red). The range of *Gaia* colours employed in each case is written in each panel. We selected G and K stars for the comparison between M35 and the Pleiades, but only K stars in the comparison with M34 due to the few data available for this cluster.

of Research MCIN/AEI/10.13039/501100011033 and No. MDM-2017-0737 Unidad de Excelencia “María de Maeztu”- Centro de Astrobiología (INTA-CSIC). Based on Clusterix 2.0 service at CAB (INTA-CSIC). This publication makes use of VOSA, maintained under the Spanish Virtual Observatory project funded by MCIN/AEI/10.13039/501100011033/ through grant PID2020-112949GB-I00. VOSA has been partially updated by using funding from the European Union’s Horizon 2020 Research and Innovation Programme, under Grant Agreement n° 776403 (EXOPLANETS-A). D.C.M. acknowledges support from a Erasmus+ grant co-funded by the European Commission and the Spanish Ministry of Education, Culture and Sport. D.C.M. thanks Dr L. Casamiquela, Dr M. Cerviño, Dr E. Marfil, Dr M. Morales-Calderón and A. Saavedra (CAB) for their comments and suggestions. M.A.A. acknowledges support from a Fulbright U.S. Scholar grant co-funded by the Nouvelle-Aquitaine Regional Council and the Franco-American Fulbright Commission. M.A.A. also acknowledges support from a Chrétien International Research Grant from the American Astronomical Society. Based on observations obtained with the Samuel Oschin Telescope 48-inch and the 60-inch Telescope at the Palomar Observatory as part of the Zwicky Transient Facility project. ZTF is supported by the National Science Foundation under Grants No. AST-1440341 and AST-2034437 and a collaboration including current partners Caltech, IPAC, the Weizmann Institute for Science, the Oskar Klein Center at Stockholm University, the University of Maryland,

Deutsches Elektronen-Synchrotron and Humboldt University, the TANGO Consortium of Taiwan, the University of Wisconsin at Milwaukee, Trinity College Dublin, Lawrence Livermore National Laboratories, IN2P3, University of Warwick, Ruhr University Bochum, Northwestern University and former partners the University of Washington, Los Alamos National Laboratories, and Lawrence Berkeley National Laboratories. Operations are conducted by COO, IPAC, and UW.

## References

- Abdelaziz, A. E., Saad, S. M., Hendy, Y. H. M., Shokry, A., & Kamal, F. Y. 2022, *New A*, 92, 101727  
 Anthony-Twarog, B. J., Deliyannis, C. P., Harmer, D., et al. 2018, *AJ*, 156, 37  
 Arancibia-Silva, J., Bouvier, J., Bayo, A., et al. 2020, *A&A*, 635, L13  
 Balaguer-Núñez, L., López del Fresno, M., Solano, E., et al. 2020, *MNRAS*, 492, 5811  
 Barrado, D., Bouy, H., Bouvier, J., et al. 2016, *A&A*, 596, A113  
 Barrado y Navascués, D., Deliyannis, C. P., & Stauffer, J. R. 2001a, *ApJ*, 549, 452

- Barrado y Navascués, D. & Stauffer, J. R. 1996, *A&A*, 310, 879
- Barrado y Navascués, D., Stauffer, J. R., Bouvier, J., & Martín, E. L. 2001b, *ApJ*, 546, 1006
- Bayo, A., Rodrigo, C., Barrado y Navascués, D., et al. 2008, *A&A*, 492, 277
- Blanco-Cuaresma, S., Soubiran, C., Heiter, U., & Jofré, P. 2014, *A&A*, 569, A111
- Boesgaard, A. M. & Friel, E. D. 1990, *ApJ*, 351, 467
- Bouvier, J. 2008, *A&A*, 489, L53
- Bouvier, J. 2020, *Mem. Soc. Astron. Italiana*, 91, 39
- Bouvier, J., Barrado, D., Moraux, E., et al. 2018, *A&A*, 613, A63
- Bouvier, J., Lanzafame, A. C., Venuti, L., et al. 2016, *A&A*, 590, A78
- Bouy, H., Bertin, E., Barrado, D., et al. 2015, *A&A*, 575, A120
- Cantat-Gaudin, T. & Anders, F. 2020, *A&A*, 633, A99
- Castelli, F., Gratton, R. G., & Kurucz, R. L. 1997, *A&A*, 318, 841
- Castelli, F. & Kurucz, R. L. 2003, in *Modelling of Stellar Atmospheres*, ed. N. Piskunov, W. W. Weiss, & D. F. Gray, Vol. 210, A20
- Castro, M., Vauclair, S., Richard, O., & Santos, N. C. 2009, *A&A*, 494, 663
- Curtis, J. L., Agüeros, M. A., Matt, S. P., et al. 2020, *The Astrophysical Journal*, 904, 140
- Deacon, N. R. & Kraus, A. L. 2020, *MNRAS*, 496, 5176
- Dumont, T., Charbonnel, C., Palacios, A., & Borisov, S. 2021, *A&A*, 654, A46
- Gaia Collaboration, Babusiaux, C., van Leeuwen, F., et al. 2018, *A&A*, 616, A10
- Gaia Collaboration, Brown, A. G. A., Vallenari, A., et al. 2021, *A&A*, 649, A1
- Gaia Collaboration, Vallenari, A., Brown, A. G. A., et al. 2023, *A&A*, 674, A1
- Galindo-Guil, F. J., Barrado, D., Bouy, H., et al. 2022, *A&A*, 664, A70
- Gebran, M. & Monier, R. 2008, *A&A*, 483, 567
- Gondoin, P. 2014, *A&A*, 566, A72
- Gray, R. O. & Corbally, C. J. 1994, *AJ*, 107, 742
- Gustafsson, B., Edvardsson, B., Eriksson, K., et al. 2008, *A&A*, 486, 951
- Heiter, U., Lind, K., Bergemann, M., et al. 2021, *A&A*, 645, A106
- Hodges, J. L. 1958, *Arkiv for Matematik*, 3, 469
- Ianna, P. A. & Schlemmer, D. M. 1993, *AJ*, 105, 209
- Jeffries, R. D., Jackson, R. J., Sun, Q., & Deliyannis, C. P. 2021, *MNRAS*, 500, 1158
- Kervella, P., Arenou, F., & Thévenin, F. 2022, *A&A*, 657, A7
- Koch, D. G., Borucki, W. J., Basri, G., et al. 2010, *ApJ*, 713, L79
- Kurucz, R. L. 1992, in *The Stellar Populations of Galaxies*, ed. B. Barbuy & A. Renzini, Vol. 149, 225
- Leiner, E. M., Mathieu, R. D., Gosnell, N. M., & Geller, A. M. 2015, *AJ*, 150, 10
- Libralato, M., Bedin, L. R., Nardiello, D., & Piotto, G. 2016, *MNRAS*, 456, 1137
- Lind, K., Asplund, M., & Barklem, P. S. 2009, *A&A*, 503, 541
- Marigo, P., Girardi, L., Bressan, A., et al. 2017, *ApJ*, 835, 77
- Martín, E. L., Basri, G., Pavlenko, Y., & Lyubchik, Y. 2002, *ApJ*, 579, 437
- Martos, G., Meléndez, J., Rathsam, A., & Carvalho Silva, G. 2023, *MNRAS*, 522, 3217
- Masci, F. J., Laher, R. R., Rusholme, B., et al. 2019, *Publications of the Astronomical Society of the Pacific*, 131, 018003
- Meibom, S., Mathieu, R. D., & Stassun, K. G. 2009, *ApJ*, 695, 679
- Meynet, G., Mermilliod, J. C., & Maeder, A. 1993, *A&AS*, 98, 477
- Nardiello, D., Bedin, L. R., Nascimbeni, V., et al. 2015, *MNRAS*, 447, 3536
- Pecaut, M. J. & Mamajek, E. E. 2013, *ApJS*, 208, 9
- Rebolo, R., Martín, E. L., Basri, G., Marcy, G. W., & Zapatero-Osorio, M. R. 1996, *ApJ*, 469, L53
- Rebolo, R., Martín, E. L., & Magazzu, A. 1992, *ApJ*, 389, L83
- Schuler, S. C., King, J. R., Fischer, D. A., Soderblom, D. R., & Jones, B. F. 2003, *AJ*, 125, 2085
- Siess, L. & Livio, M. 1997, *ApJ*, 490, 785
- Snedden, C., Bean, J., Ivans, I., Lucatello, S., & Sobeck, J. 2012, *MOOG: LTE line analysis and spectrum synthesis*, *Astrophysics Source Code Library*, record ascl:1202.009
- Soares-Furtado, M., Hartman, J. D., Bhatti, W., et al. 2020, *ApJS*, 246, 15
- Soderblom, D. R., Hillenbrand, L. A., Jeffries, R. D., Mamajek, E. E., & Naylor, T. 2014, in *Protostars and Planets VI*, ed. H. Beuther, R. S. Klessen, C. P. Dullemond, & T. Henning, 219–241
- Soderblom, D. R., Jones, B. F., Balachandran, S., et al. 1993, *AJ*, 106, 1059
- Somers, G. & Pinsonneault, M. H. 2014, *ApJ*, 790, 72
- Somers, G. & Pinsonneault, M. H. 2015, *MNRAS*, 449, 4131
- Stauffer, J. R., Barrado y Navascués, D., Bouvier, J., et al. 1999, *ApJ*, 527, 219
- Stauffer, J. R., Schultz, G., & Kirkpatrick, J. D. 1998, *ApJ*, 499, L199
- Steinhauer, A. & Deliyannis, C. P. 2004, *ApJ*, 614, L65
- Taylor, M. B. 2005, in *Astronomical Society of the Pacific Conference Series*, Vol. 347, *Astronomical Data Analysis Software and Systems XIV*, ed. P. Shopbell, M. Britton, & R. Ebert, 29
- Ziegler, C., Tokovinin, A., Briceño, C., et al. 2020, *AJ*, 159, 19